### A TALE OF TWO (VISCO)CITIES

# Electromagnetic Turbulence and Transport Bifurcations: Implications for next-generation Fusion Power Plants

D. Kennedy<sup>1,2</sup>, Y. Zhang<sup>2,3</sup>, P.G. Ivanov<sup>1,2</sup>, T. Adkins<sup>4</sup>, F.J. Casson<sup>1</sup>, H.G. Dudding<sup>1</sup>, B.S. Patel<sup>1</sup>, C.M. Roach<sup>1</sup>, and H.R. Wilson<sup>5</sup>

Email: daniel.kennedy@ukaea.uk

#### **ABSTRACT**

The nonlinear transition to large heat fluxes in local gyrokinetic simulations of electromagnetic turbulence in STEP (a conceptual spherical tokamak power plant) is investigated. Consistent with results reported elsewhere, the onset of enhanced transport is shown to depend on a critical value of  $q^2\beta_e$  and appears closely connected to a limit on  $\beta_{\rm pol}$ . A broad set of simulations demonstrates that the transition is mediated by the competition between  $E \times B$  and magnetic-flutter momentum fluxes. Access to a second-stable regime allows a return to more modest fluxes at higher  $\beta'$ . The ideal ballooning mode (IBM) threshold is identified as a useful proxy for charting these regions of parameter space. These findings establish a predictive framework for recognising "no-go" zones in local gyrokinetics and provide new insight into the saturation physics of electromagnetic turbulence in STEP and potentially in other high- $q^2\beta_e$  devices.

### 1. INTRODUCTION

The performance of magnetic-confinement-fusion (MCF) devices, such as spherical tokamaks (STs), is often limited by turbulent fluctuations, which dominate losses of heat, particles, and momentum. Predicting turbulence-driven transport is therefore essential for optimising future STs. The UK STEP fusion programme [1] aims to develop a compact power plant generating over 100 MW of net electric power, based on the ST concept. STEP is expected to operate at significantly higher values of plasma  $\beta_e$ —the ratio of plasma (electron) pressure to magnetic pressure—than conventional-aspect-ratio present-day machines [2], where electromagnetic (EM) effects are predicted to strongly influence turbulent transport. In such regimes, local gyrokinetic (GK) simulations provide a first-principles framework capable of capturing the relevant dynamics and are increasingly relied upon to guide scenario development.

The first GK analysis of one of STEP's reference flat-top operating points, STEP-EC-HD [3], was conducted in [4]. This study identified unstable *hybrid* kinetic ballooning modes (hKBMs)—which combine features of kinetic ballooning modes (KBMs), ion-temperature-gradient-driven modes (ITGs), and trapped-electron modes (TEMs)—as the dominant instabilities, with subdominant microtearing modes (MTMs) also present. Subsequent nonlinear simulations [5, 6] revealed that, in the absence of equilibrium flow shear, hKBM-driven turbulence can generate particle and heat fluxes far exceeding the available heating and fuelling rates. Simulations of STEP's reference flat-top operating points are often difficult to saturate, with phases of apparent saturation punctuated by transient bursts of transport and a transition to extreme heat fluxes. However, it was also shown in [5] that in scans where  $\beta' \propto \beta_e$  saturation at reasonable fluxes is possible at both larger and smaller values of  $\beta_e$ .

Figure 1 shows the turbulent heat flux from local gyrokinetic GENE [7] calculations at various  $\beta_e$  values, with  $\beta'$  scaled such that  $\beta' \propto \beta_e$ . Simulations correspond to a mid-radius surface of the STEP-EC-HD variant studied

<sup>&</sup>lt;sup>1</sup>United Kingdom Atomic Energy Authority (UKAEA Group), Abingdon, UK

<sup>&</sup>lt;sup>2</sup>Rudolf Peierls Centre for Theoretical Physics, University of Oxford, Oxford UK

<sup>&</sup>lt;sup>3</sup>St Edmund Hall College, Oxford, UK

<sup>&</sup>lt;sup>4</sup>Tokamak Energy Ltd, Abingdon UK

<sup>&</sup>lt;sup>5</sup>Princeton Plasma Physics Laboratory, Princeton, USA

<sup>&</sup>lt;sup>6</sup>UK Industrial Fusion Solution Ltd. (UKAEA Group), Abingdon, UK

<sup>&</sup>lt;sup>1</sup>All simulations in this paper are local simulations; i.e., they are performed in a domain whose perpendicular size is infinitesimal compared with the equilibrium scale lengths, which are taken to be constant across the domain.

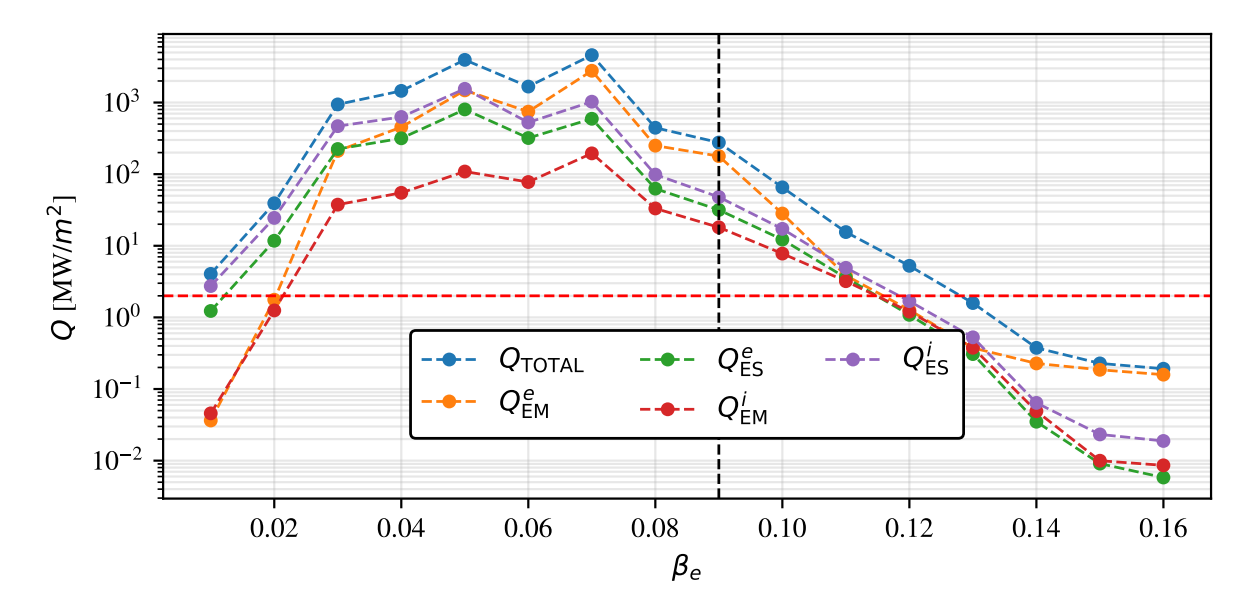


FIG. 1. Electrostatic and electromagnetic electron and ion heat fluxes as functions of  $\beta_e$  from nonlinear simulations using GENE. In this work, the pressure gradient,  $\beta'$ , is always scaled  $\propto \beta_e$ . Simulations are shown for a mid-radius surface in an early design of STEP-EC-HD examined in [4, 5] where the nominal value of  $\beta_e$  is given by the black dashed line. The red horizontal line denotes the available heating power.

in [4, 5], use identical parameters to [5], and omit equilibrium flow shear<sup>2</sup>. The black dashed line indicates the consistent  $\beta_e$  for this flux-surface, while the red dashed line marks the available heating power. Two transitions are observed: a sharp increase in heat flux by two orders of magnitude at  $\beta_e \in [0.02, 0.03]$ , and a smoother reduction at  $\beta_e > 0.10$ . This work focuses on analysing these transitions, with the eventual aim of identifying gyrokinetic "no-go" zones and assessing viable operating points [8].

#### 1.1. Non-zonal transition

Similar nonlinear behaviour to that found in STEP has long been reported in electromagnetic simulations of ITG-driven turbulence, where at finite  $\beta_e$  the system can undergo an *electromagnetic runaway* [9]. In these cases, simulations that initially appear saturated lose regulation and develop extreme transport, a transition not tied to any linear instability threshold. Following [9], this first transition is referred to as the *non-zonal transition*, marking the suppression of zonal flow activity. Explanations for the non-zonal transition include disruption of zonal flows and magnetic stochasticity, while more recent work has attributed the transition to a cancellation between  $E \times B$  and magnetic-flutter stresses [10]. A hallmark of this regime is the appearance of streamer-like radial structures that efficiently transport heat and are incompatible with zonal flows. The present study (see also [11, 8]) focuses on identifying the  $\beta_e$  threshold for this non-zonal transition in STEP and exploring whether it can be moderated.

Recent work by Zhang et al. [11] shows that the non-zonal transition in nonlinear GK simulations occurs when magnetic-flutter stress extracts energy from zonal flows faster than it is injected by  $E \times B$  stress, leading to weak zonal flows and elevated transport. The transition was demonstrated across multiple geometries, with the critical value of  $q^2\beta_e$  (above which the transition occurs) found to depend on device and equilibrium shaping. A practical estimate of this threshold was proposed, based on the observation that the stress ratio scales as  $(q^2\beta_e)^2$  at low  $\beta_e$ , enabling extrapolation of the transition boundary from a single nonlinear simulation. Building on the Zhang et al. [11] framework, this paper (see also [6]) extends the analysis to STEP, emphasising the role of second-stability enabling a return to more modest fluxes at larger  $q^2\beta_e$ , and examining the usefulness of the ideal ballooning mode (e.g., [12]) as a proxy for the transition boundary.

## 2. ZONAL ENERGY BALANCE AND NONLINEAR THRESHOLD OF ZHANG ET AL. [11]

We begin by summarising the coordinate conventions used in [11]. The equilibrium magnetic field is expressed in Clebsch form,  $\mathbf{B} = \nabla \alpha \times \nabla \psi$ , with  $\psi$  labelling flux surfaces (e.g. poloidal magnetic flux, set to zero on-axis)

<sup>&</sup>lt;sup>2</sup>STEP is expected to have minimal external momentum injection.

and  $\alpha = \zeta - q(\psi)\theta$  labelling fieldlines within a surface (e.g., [13]). To work in the local, flux-tube approximation [14], we adopt field-aligned coordinates (x, y, z), where

$$x = \frac{\mathrm{d}x}{\mathrm{d}\psi}(\psi - \psi_0), \qquad y = \frac{\mathrm{d}y}{\mathrm{d}\alpha}(\alpha - \alpha_0), \tag{1}$$

denote radial and binormal displacements, and z is the coordinate along the fieldline. These coordinates are defined so that  $\mathbf{B}/B_0 = \nabla x \times \nabla y$ , where x and y have units of length ( $B_0$  is a reference magnetic-field strength).

In axisymmetry, equilibrium quantities are independent of y, so fluctuations may be expanded as

$$g(\mathbf{r}) = \sum_{\mathbf{k}_{\perp}} g_{\mathbf{k}_{\perp}}(z) e^{i(k_x x + k_y y)}, \qquad (2)$$

with statistical periodicity assumed in the perpendicular plane.

Zonal perturbations (constant on a flux-surface) are naturally extracted using the flux-surface average

$$\langle \dots \rangle_{\psi} = \lim_{\Delta \psi \to 0} \frac{1}{\Delta V(\psi)} \int_{\Delta V(\psi)} (\dots) d^3 r, \qquad \Delta V(\psi) = V(\psi + \Delta \psi) - V(\psi). \tag{3}$$

In [11] it was shown from the quasineutrality equation that the zonal fields in an electromagnetic plasma evolve according to

$$\frac{\partial}{\partial t} \left\langle \sum_{\mathbf{k}_{\perp}} e^{i\mathbf{k}_{\perp} \cdot \mathbf{r}} \left[ \sum_{s} \frac{q_{s}^{2} n_{s}}{T_{s}} (1 - \Gamma_{0s}) \phi_{\mathbf{k}_{\perp}} - \sum_{s} q_{s} n_{s} \Gamma_{1s} \frac{\delta B_{\parallel \mathbf{k}_{\perp}}}{B} \right] \right\rangle_{\psi} = \Pi_{\text{lin}} + \Pi_{\text{turb}}, \tag{4}$$

where the LHS represents the flux-surface-averaged time evolution of the generalised polarisation charge, including electrostatic and magnetic compressibility effects, while the RHS includes linear and nonlinear (turbulence-driven) contributions to the divergence of the radial flux surface averaged current density . Here  $\phi$  is the perturbed electrostatic potential,  $A_{\parallel}$  is the component of the vector potential parallel to the equilibrium field,  $\delta B_{\parallel}$  is the perturbation of the magnetic field parallel to B, and  $h_s$  is the non-adiabatic part of the perturbed distribution function, defined in guiding centre space by  $\delta f_s = -(q_s\phi/T_s)F_s + h_s$  for species s with equilibrium distribution  $F_s$ , charge  $q_s$ , density  $n_s$ , and temperature  $T_s$ . The functions  $\Gamma_{0s}(\alpha_s) = I_0(\alpha_s)e^{-\alpha_s}$  and  $\Gamma_{1s}(\alpha_s) = [I_0(\alpha_s) - I_1(\alpha_s)]e^{-\alpha_s}$  are finite-Larmor-radius operators, where  $\alpha_s = \frac{1}{2}(k_{\perp}\rho_s)^2$ ,  $\rho_s = v_{\text{ths}}/|\Omega_s|$  is the species Larmor radius,  $v_{\text{ths}} = \sqrt{2T_s/m_s}$  is the thermal speed, and  $\Omega_s = q_s B/(m_s c)$  is the cyclotron frequency. The electromagnetic fields appearing in (4) are determined by quasineutrality and Ampère's law,

$$\sum_{s} \frac{q_s^2 n_s}{T_s} \phi = \sum_{s} q_s \int d^3 \boldsymbol{v} \langle h_s \rangle_{\boldsymbol{r}}, \tag{5}$$

$$\nabla_{\perp}^{2} A_{\parallel} = -\frac{4\pi}{c} \sum_{s} q_{s} \int d^{3}\boldsymbol{v} \, v_{\parallel} \langle h_{s} \rangle_{\boldsymbol{r}}, \quad \nabla_{\perp}^{2} \delta B_{\parallel} = -\frac{4\pi}{c} \, \mathbf{b} \cdot \left[ \nabla_{\perp} \times \sum_{s} q_{s} \int d^{3}\boldsymbol{v} \, \langle \boldsymbol{v}_{\perp} h_{s} \rangle_{\boldsymbol{r}} \right], \tag{6}$$

where  $v_{\parallel}$  and  $v_{\perp}$  are particle velocity components parallel and perpendicular to the equilibrium field,  $\mathbf{b} = \mathbf{B}/B$ , c is the speed of light, and the gyroaverage  $\langle \dots \rangle_r$  denotes averaging over gyrophase at fixed particle position.

The first term on the right-hand-side of (4) is the linear contribution to the divergence of the perturbed radial current.

$$\Pi_{\text{lin}} \equiv -\left\langle \sum_{s} q_{s} \int d^{3} \boldsymbol{v} \left[ (\boldsymbol{v}_{ds} \cdot \nabla x) \left\langle \frac{\partial h_{s}}{\partial x} \right\rangle_{\boldsymbol{r}} \right] + \sum_{s'} \left\langle \left\langle C_{ss'}^{(l)}[h_{s}] \right\rangle_{\boldsymbol{R}_{s}} \right\rangle_{\boldsymbol{r}} \right\rangle_{\psi},$$
(7)

that describes the (radial) drifting of the plasma across flux-surfaces due to the magnetic drifts and the effects of inter-particle collisions on the gyrokinetic distribution function  $h_s$  through the (linearised) collision operator  $C_{ss'}^{(l)}$ .

The turbulent (nonlinear) contribution to the divergence of the perturbed radial current in (4) can be written as

$$\Pi_{\text{turb}} = -\left\langle \sum_{s} q_{s} \int d^{3} \boldsymbol{v} \left\langle \boldsymbol{v}_{\chi} \cdot \nabla h_{s} \right\rangle_{\boldsymbol{r}} \right\rangle_{\psi}, \qquad \boldsymbol{v}_{\chi} \equiv \frac{c}{B} \mathbf{b} \times \frac{\partial \langle \chi \rangle_{\boldsymbol{R}_{s}}}{\partial \boldsymbol{R}_{s}}, \quad \chi = \phi - \frac{\mathbf{v} \cdot \mathbf{A}}{c},$$
(8)

with contributions conventionally separated into the  $E \times B$  term  $\Pi_{\phi}$ , the magnetic-flutter term  $\Pi_{A_{\parallel}}$ , and the compressive term  $\Pi_{\delta B_{\parallel}}$ .

#### IAEA-CN-392/3074 CONFERENCE PREPRINT

#### 2.1. Zonal energy balance

Following [11], we recast (4) as an energy equation (see details in [11]). Neglecting the small  $\delta B_{\parallel}$  contribution on the LHS, and focusing on large-scale zonal flows with  $k_x \rho_i \ll 1$ , the ion polarisation terms simplify as  $1 - \Gamma_0 \simeq \frac{1}{2} k_x^2 \rho_i^2$  and  $\Gamma_1 \simeq \frac{1}{4} k_x^2 \rho_i^2$ , so the zonal-flow inertia reduces to quadratic dependence on  $k_x$ . Because x is a flux coordinate, the physical perpendicular wavenumber is  $k_{\perp} = k_x |\nabla x|$ . In this limit, the zonal energy balance (per  $k_x$  mode) then reads

$$\partial_t E_{\rm ZF}(k_x) \equiv \frac{Z^2 n_e |\nabla x|^2}{4T_i} \, \partial_t \left| \langle \phi \rangle_{\psi, k_x} \right|^2 = -\nu_{\text{lin}, k_x} - \nu_{\phi, k_x} - \nu_{A_{\parallel}, k_x} - \nu_{\delta B_{\parallel}, k_x} \equiv -\nu_{\rm ZF, k_x}, \tag{9}$$

where the  $\nu_{{\rm ZF},k_x}$  is the turbulent ZF damping term and the different channels are

$$\nu_{\text{lin},k_x} = -\text{Re}\left(\langle \phi \rangle_{\psi,k_x}^* \Pi_{\text{lin},k_x}\right),\tag{10}$$

$$\nu_{\phi,k_x} = -\text{Re}\left(\langle \phi \rangle_{\psi,k_x}^* \Pi_{\phi,k_x}\right),\tag{11}$$

$$\nu_{A_{\parallel},k_x} = -\text{Re}\left(\langle \phi \rangle_{\psi,k_x}^* \Pi_{A_{\parallel},k_x}\right),\tag{12}$$

$$\nu_{\delta B_{\parallel},k_{x}} = -\text{Re}\left(\langle \phi \rangle_{\psi,k_{x}}^{*} \Pi_{\delta B_{\parallel},k_{x}}\right). \tag{13}$$

Thus the zonal polarisation energy evolves through a competition between a linear term and the three nonlinear transfer channels. In strongly electromagnetic regimes relevant to STEP, the turbulent contributions often dominate, particularly during electromagnetic runaway when the heat flux grows rapidly [5, 6]. The sign and persistence of the different terms (and their sum) on the RHS of (9) therefore provide a criterion for zonal saturation. In saturated turbulence, the RHS of (9) should be close to zero, a net-positive RHS strengthens zonal flows, while a net-negative RHS damps them, leading to streamer-dominated states with elevated fluxes.

#### 2.2. Threshold for the non-zonal transition

In [11], the authors argue that the critical plasma beta,  $q^2\beta_e=C_{\rm nl}$ , above which electromagnetic turbulence will fail to saturate, arises from the competition between electrostatic and electromagnetic (Alfvénic) dynamics (in particular, that the sign of  $\nu_{\rm ZF},k_x$  is set by competition between the  $\nu_{\phi,k_x}$  and  $\nu_{A_\parallel,k_x}$ , which tend to have the opposite sign). At low beta, the Alfvén speed  $v_A \sim v_{\rm thi}/\sqrt{\beta}$ , so magnetic perturbations are rapidly smoothed by Alfvén-wave propagation. This prevents the magnetic-flutter stress from contributing significantly to zonal-flow dynamics, leaving saturation governed primarily by  $E\times B$  effects. However, as  $\beta_e$  increases,  $v_A$  decreases and electromagnetic effects become dynamically relevant. Specifically, this happens when the Alfvén frequency for the lowest parallel wavenumber mode,  $\omega_A^{\rm min} \sim v_A/(qR)$ , becomes comparable to the MHD interchange growth rate  $\gamma_{\rm MHD} \sim v_{\rm thi}/\sqrt{RL_{T_i}}$ . Equating these two timescales yields a critical beta,

$$\beta_e^{\text{crit}} \sim \frac{L_{T_i}}{q^2 R},$$
 (14)

which marks the threshold above which Alfvénic perturbations can interact strongly with drift waves on comparable timescales, allowing magnetic flutter and its associated stresses to influence the turbulence.<sup>3</sup>.

The  $\beta_e$  limit in (14) can be related to a limit on  $\beta_{\rm pol} \sim q^2\beta_e(R/a)^2$  [8]. Again,  $\beta_{\rm pol}$  becoming order unity marks the onset of Alfvénic dynamics. In the large-aspect-ratio limit, the ratio of perpendicular to parallel current divergence scales as  $\nabla \cdot \mathbf{J}_{\perp}/\nabla \cdot \mathbf{J}_{\parallel} \propto \beta_e(qR/a)^2$ , so changes in  $\beta_e$ ,  $q^2$ , or  $(R/a)^2$  have equivalent impact in driving the system into a non-zonal regime [8]. This means that the limit occurs at a lower value of beta (toroidal) in conventional-aspect-ratio devices, while tighter-aspect-ratio configurations are naturally more resilient at high  $\beta_e$  (for fixed q). In practice, however, local gyrokinetic simulations are typically performed at fixed aspect ratio, so the threshold is most usefully expressed in terms of the control parameter  $q^2\beta_e$ . We begin our investigation

by verifying whether the theory developed in [11] also explains the non-zonal transition observed in gyrokinetic simulations of STEP-EC-HD (Section 3.1). We then show that turbulence mitigation is possible at larger values of  $q^2\beta_e$  when  $\beta'$  is scaled  $\propto \beta_e$  (Section 3.2).

<sup>&</sup>lt;sup>3</sup>The estimate (14) can also be derived directly from quasilinear estimates of the terms on the right-hand-side of (4) See Appendix B of [11].

#### 3. NUMERICAL SIMULATIONS OF STEP-EC-HD

The simulations presented in here focus on a single equilibrium flux surface near mid-radius ( $q=3.5, \Psi_n=0.49$ ) in the STEP reference scenario STEP-EC-HD<sup>1</sup>, where EC denotes electron cyclotron heating and current drive, and HD denotes high density. This scenario is an early iteration of the STEP design concept, targeting a fusion power of  $P_{\rm fus}=1.7$  GW. The same flux surface has been studied previously [4, 5, 6], and is chosen here to enable direct comparison. All parameter scans are performed with this surface as the reference.

The GK analysis presented in the paper employed pyrokinetics [15]. For the simulations reported here, a Miller parameterisation [16] of the local magnetic equilibrium geometry was generated, with shaping parameters fitted to the chosen surface. Table 1 lists key local equilibrium quantities, including magnetic shear  $\hat{s}$ , safety factor q, normalised minor radius  $\rho/a$ , elongation  $\kappa$  and  $\kappa'$ , triangularity  $\delta$  and  $\delta'$ , the Shafranov shift derivative  $\Delta'$ , and the normalised inverse density and temperature gradient scale lengths  $a/L_{ns}$  and  $a/L_{Ts}$ . The binormal wavenumber  $k_y^{n=1}\rho_s$  corresponds to toroidal mode number n=1. The simulations evolve two species—electrons and a deuterium—tritium mix—while neglecting impurities and fast particles.

TABLE 1. LOCAL PARAMETERS FOR THE MID-RADIUS SURFACE IN THE STEP-EC-HD CONFIGURATION.

Parameter	Value	Parameter	Value
$\beta_e$	0.09	$\beta'$	-0.48
q	3.5	$\hat{s}$	1.20
$\Psi_n$	0.49	$\rho = r/a$	0.64
$\kappa$	2.56	$\kappa'$	0.06
$\delta$	0.29	$\delta'$	0.46
$\Delta'$	-0.40	$k_y^{n=1}\rho_s$	0.0047
$a/L_{n_e}$	1.06	$a/L_{T_e}$	1.58
$a/L_{n_i}$	1.06	$a/L_{T_i}$	1.82

The diagnostics of [11], implemented in the gyrokinetic code stella [17], are used to quantify zonal-flow dynamics across the transition boundary. We use stella to calculate the zonal-flow damping terms, complex in  $k_x$  and t. As shown in [11], the dominant contribution to the ZF damping terms arise from the largest scales, reflecting that zonal flows suppress turbulence most effectively at scales larger than the outer scale. Large-scale viscosities are therefore defined, for example, as

$$\nu_{\phi} = \sum_{|k_x| < k_{y0}} \nu_{\phi, k_x},\tag{15}$$

with  $k_{y0}$  the outer scale of the turbulence, i.e. the peak of the heat flux spectrum in  $k_y$ .

stella employs spatial coordinates  $(k_x,k_y,z)$  and velocity-space coordinates  $(v_{\parallel},\mu)$ , identical to the discretisation in GENE, enabling direct comparison. Over 100 nonlinear simulations (and over 1000 linear simulations) were performed. Table 2 lists the nominal resolution parameters:  $n_{k_x}$  is the spectral radial resolution,  $n_{k_y}$  the number of binormal Fourier modes,  $n_z$  the number of grid points along the field line,  $n_{v_{\parallel}}$  and  $n_{\mu}$  the velocity-space resolutions, and  $k_y^{\min}$  ( $k_x^{\min}$ ) the smallest non-zonal binormal (radial) wavenumber evolved in the simulation. The chosen grids are comparable to those used in earlier STEP-EC-HD studies [5, 6]. Collisions are modelled with the Dougherty operator [17]. The radial box size is set as  $L_x = j/(\hat{s}k_{y,\min})$  with j=8 to include eight rational surfaces of the lowest toroidal mode number [5].

TABLE 2. NOMINAL RESOLUTION PARAMETERS FOR LINEAR (L) AND NONLINEAR (NL) SIMULATIONS

Simulation	$n_{k_x}$	$n_{k_y}$	$n_z$	$n_{v_\parallel}$	$n_{\mu}$	$k_x^{\min}$	$k_y^{\mathrm{min}}$
L	5	1	64	32	16	_	_
NL	128	32	32	32	16	0.025	0.025

<sup>&</sup>lt;sup>1</sup>SimDB UUID: 2bb77572-d832-11ec-b2e3-679f5f37cafe, Alias: smars/jetto/step/88888/apr2922/seq-1

# 3.1. Forward transition to extreme heat fluxes with increasing $\beta_e$ ; competition between E $\times$ B nonlinear term and magnetic flutter nonlinear term defines a "no-go zone" for local gyrokinetics

Figure 2 (**LHS**) summarises a parameter scan over the  $(q,\beta_e)$  plane (where  $\beta' \propto \beta_e$ ) using 128 nonlinear gyrokinetic simulations of the STEP-EC-HD equilibrium performed with stella. Simulations that saturate with  $Q_{\rm total} < 100~{\rm MW/m^2}$  are marked by blue crosses, while red crosses denote cases where the heat flux continued to rise with no sign of saturation. The threshold of  $200~{\rm MW/m^2}$  is arbitrary, chosen to represent an order-of-magnitude increase relative to the well-saturated low- $\beta_e$  regime; in practice the transition is sharp, corresponding to a steep increase in  $dQ_{\rm total}/d\beta_e$ . The black dashed line shows the ideal ballooning mode (IBM) threshold computed with the pyrokinetics solver based on the approach used in [18], while the solid line corresponds to the predicted nonlinear boundary  $q^2\beta_e = C_{\rm nl}^{\rm STEP}$  calculated using the approach proposed in [11], with  $C_{\rm nl}^{\rm STEP}$  determined by fitting a single reference case at  $(q,\beta_e)=(3.5,0.026)$ . The close agreement between this prediction and the observed transition supports the relevance of the  $q^2\beta_e$  criterion and delineates a local GK "no-go zone" (red crosses) where fluxes are very large. The reference STEP-EC-HD operating point,  $(q,\beta_e)=(3.5,0.09)$  [black box], lies within this region. All simulations were performed without equilibrium flow shear, noting the absence of external momentum injection in STEP-EC-HD (although intrinsic flows are likely and simulations do predict flow shear can reduce fluxes significantly [5]). Figure 2 (**RHS**) zooms in on the dashed box, showing runs close to the threshold. Green numbers indicate the ratio of  $|\nu_{A_{\parallel}}|/|\nu_{\phi}|$ , which is seen to cross unity as predicted in [11].

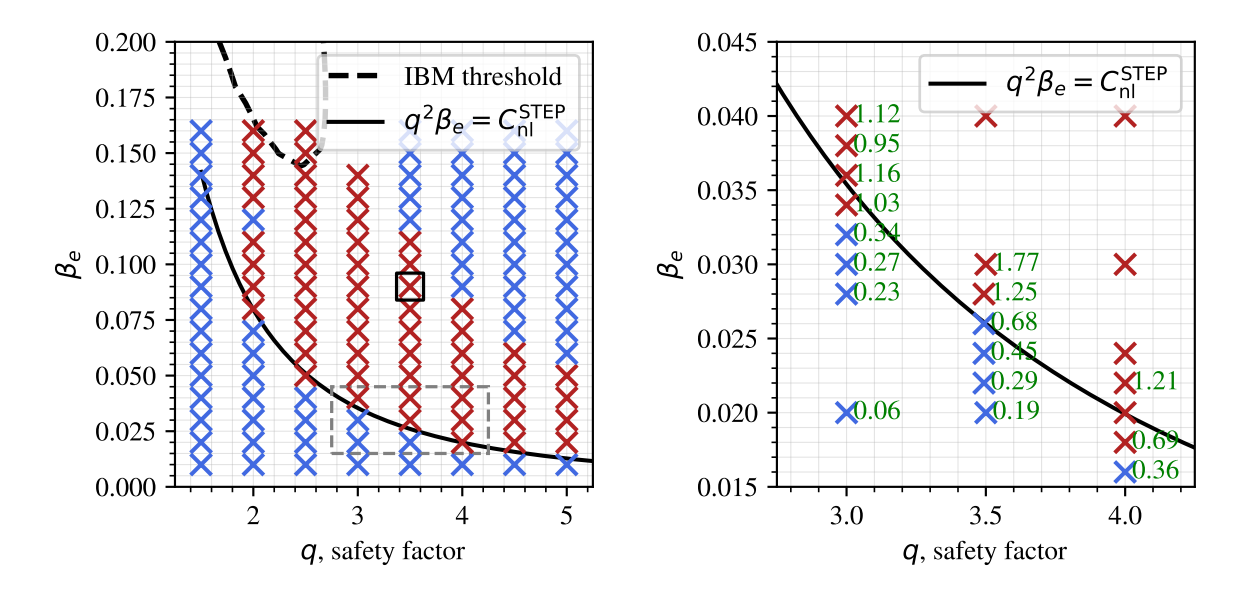


FIG. 2. (**LHS**) Results from nonlinear simulations of STEP-EC-HD at various values of q and  $\beta_e$  using stella. Apart from  $\beta'$ , which is always proportional to  $\beta_e$ , all other local parameters are fixed. Simulations that converge to  $Q_{\rm total} < 100 \, {\rm MW \, m^{-2}}$  are marked by blue crosses. Simulations that do not converge to this threshold within the simulated timescale are marked by red crosses (see text for details). The dashed black line shows the ideal ballooning mode threshold calculated with pyrokinetics. The solid black line is the predicted transition curve  $q^2\beta_e = C_{\rm nl}^{\rm STEP}$  [11], where  $C_{\rm nl}^{\rm STEP}$  is obtained by fitting a single simulation at  $(q,\beta_e) = (3.5,0.026)$ . The black box marks the nominal STEP-EC-HD operating point. (RHS) Zoom of the region marked by the dashed box in the LHS, highlighting multiple simulations near the observed threshold. Green numbers indicate the ratio of magnetic-flutter to  $E \times B$  viscosity.

# 3.2. Reverse transition to lower heat fluxes with increasing $\beta_e$ ; the role of $\beta'$ stabilisation and access to second stability

Nonlinear simulations of STEP and Cyclone-Base-Case geometries reveal the existence of a reverse transition to reduced heat fluxes at large values of  $q^2\beta'$ . This behaviour is associated with the stabilisation of the hybrid kinetic ballooning mode (hKBM) at large  $\beta'$  and the emergence of microtearing modes as the dominant linear instability, consistent with the  $\beta'$ -stabilisation mechanism [19]. Linear calculations (Figure 3, LHS) demonstrate that the growth rate of the hKBM decreases as  $\beta_e$  increases, enabling the recovery of zonal regulation and a return to moderate flux levels despite the large value of  $q^2\beta_e$ .

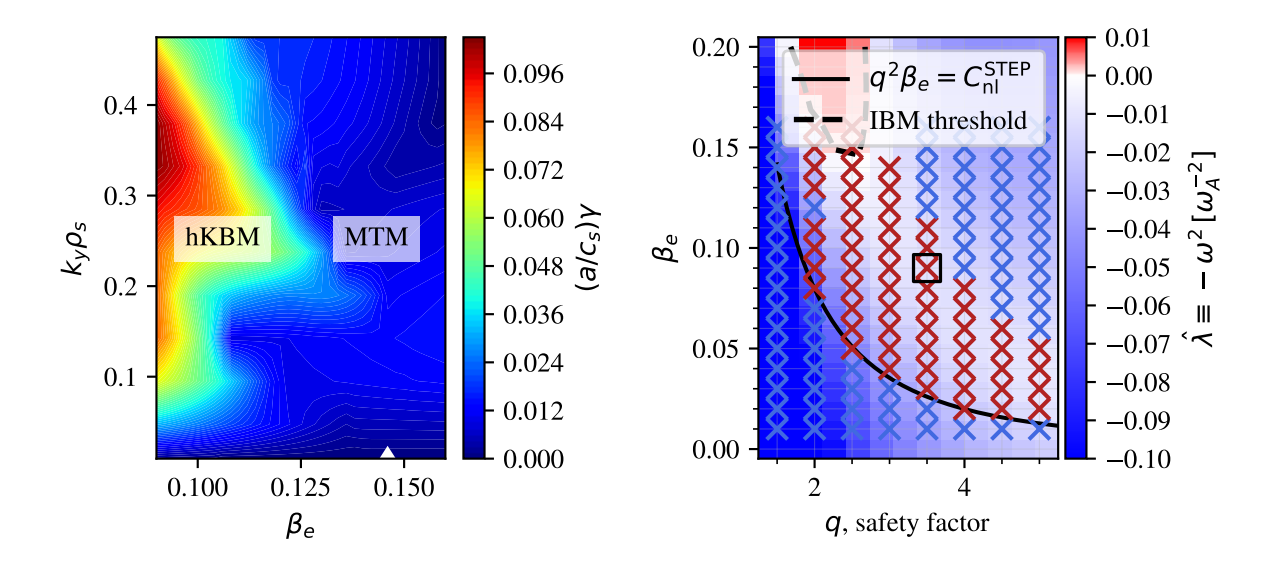


FIG. 3. Growth rate (**LHS**) of the fastest growing linear mode as a function of  $k_y \rho_s$  and  $\beta_e$  from GENE linear simulations of STEP-EC-HD for fixed q=3.5. The values of  $\beta_e$  cover the reverse transition observed in Figure 2. There is a transition in the dominant instability across the reverse transition from hKBM to MTM. (**RHS**) growth rate (positive) and real frequency (negative) of the ideal ballooning mode overplotted on the nonlinear data of Figure 2. Isolines of the IBM eigenvalue (see text) track the shape of the second-stable region where simulations saturate at more modest fluxes (upper right corner).

The ideal ballooning mode (IBM) eigenvalue,  $\hat{\lambda} \equiv -\omega^2$ , is obtained from the ballooning mode equation and quantifies the competition between pressure-gradient drive and field-line bending (e.g., [12]). Positive values correspond to instability (exponentially growing ballooning modes), while negative values indicate stability (oscillatory modes), with more negative values denoting stronger Alfvénic restoring forces and greater distance from the IBM instability boundary. Because the same Alfvénic field-line bending physics underlies the magnetic-flutter stress in gyrokinetics,  $\hat{\lambda}$  provides a natural link between linear MHD stability and the nonlinear stress balance that governs saturation. In practice, the IBM stability boundary, parametrised by  $\alpha_{\rm MHD} \propto q^2 \beta'$ , proves to be a useful proxy for identifying both the high-flux regime and the second-stable region (Figure 3, RHS). Although it does not accurately capture the first nonlinear transition—since the runaway occurs below the IBM threshold—it successfully tracks access to second stability and the associated reduction of turbulent fluxes. This makes the IBM eigenvalue a computationally inexpensive diagnostic for anticipating saturation behaviour, and highlights a direct connection between ideal MHD stability and nonlinear gyrokinetic turbulence in STEP.

### 4. SUMMARY

Local GK predicts the existence of a non-zonal transition to a high-flux regime, which places a clear constraint on the applicability of local gyrokinetics in STEP-like plasmas. The criterion  $q^2\beta_e > C_{\rm nl}$  can be used as a practical "no-go" condition to guide conservative scenario design. In addition the return to more modest fluxes at higher  $\beta'$  highlights the existence of a plasma state with improved confinement if there is sufficiently deep access to second-stability (for IBMs). Access to such states needs to be investigated, and the IBM proxy will provide a computationally efficient diagnostic to help guide scenario planning and optimisation.

## **ACKNOWLEDGEMENTS**

The authors would like to thank A. A. Schekochihin, M. Barnes, D. Dickinson, A. Bokshi, and M. Giacomin. This work has been funded by STEP, a major technology and infrastructure programme led by UK Industrial Fusion Solutions Ltd (UKIFS), which aims to deliver the UK's prototype fusion powerplant and a path to the commercial viability of fusion. Simulations were performed using resources provided by the EUROfusion High Performance Computer PITAGORA hosted by CINECA (Italy) under the project FUAP01-GEMST25. Part of this work was performed using resources provided by the Cambridge Service for Data Driven Discovery (CSD3) operated by the University of Cambridge Research Computing Service (www.csd3.cam.ac.uk), provided by

#### IAEA-CN-392/3074 CONFERENCE PREPRINT

Dell EMC and Intel using Tier-2 funding from the Engineering and Physical Sciences Research Council (capital grant EP/T022159/1), and DiRAC funding from the Science and Technology Facilities Council (www.dirac.ac.uk).

#### REFERENCES

- [1] H. Meyer. "Plasma burn—mind the gap". In: <u>Philosophical Transactions of the Royal Society A: Mathematical, Physical and 382.2280 (2024)</u>, p. 20230406.
- [2] S M Kaye, J W Connor, and C M Roach. "Thermal confinement and transport in spherical tokamaks: a review". In: Plasma Physics and Controlled Fusion 63.12 (2021), p. 123001.
- [3] E. Tholerus et al. "Flat-top plasma operational space of the STEP power plant". In: <u>Nuclear Fusion</u> 64.10 (2024), p. 106030.
- [4] D. Kennedy et al. "Electromagnetic gyrokinetic instabilities in STEP". In: <u>Nuclear Fusion</u> 63.12 (2023), p. 126061.
- [5] M. Giacomin et al. "On electromagnetic turbulence and transport in STEP". In: <u>Plasma Physics and Controlled Fusion</u> 66 (2024), p. 055010.
- [6] D. Kennedy et al. "On the importance of parallel magnetic-field fluctuations for electromagnetic instabilities in STEP". In: Nuclear Fusion 64.8 (2024), p. 086049.
- [7] F. Jenko et al. "Electron temperature gradient driven turbulence". In: <u>Physics of Plasmas</u> 7.5 (2000), pp. 1904–1910.
- [8] D. Kennedy et al. "On the transition to large fluxes and access to second stability in gyrokinetic simulations of electromagnetic turbulence in STEP". In preparation.
- [9] M. J. Pueschel et al. "Properties of high- $\beta$  microturbulence and the non-zonal transition". In: <u>Physics of Plasmas</u> 20.10 (2013), p. 102301.
- [10] F. Rath and A. G. Peeters. "Transport hysteresis in electromagnetic microturbulence caused by mesoscale zonal flow pattern-induced mitigation of high turbulence runaways". In: <a href="Physics of Plasmas">Physics of Plasmas</a> 29 (2022), p. 042305.
- [11] Y. Zhang et al. "On the zonal flow generation and saturation of electromagnetic ion-scale turbulence". In preparation.
- [12] R Davies, D Dickinson, and H Wilson. "Kinetic ballooning modes as a constraint on plasma triangularity in commercial spherical tokamaks". In: 64.10 (2022), p. 105001.
- [13] W. D. D'Haeseleer et al. <u>Flux Coordinates and Magnetic Field Structure</u>. Heidelberg: Springer Berlin Heidelberg, 1991.
- [14] M. A. Beer, S. C. Cowley, and G. W. Hammett. "Field-aligned coordinates for nonlinear simulations of tokamak turbulence". In: Physics of Plasmas 2.7 (1995), p. 2687.
- 9.95 (2024), p. 5866.

[15] Bhavin S. Patel et al. "Pyrokinetics - A Python library to standardise gyrokinetic analysis". In: Journal of Open Source Software

- [16] R. L. Miller et al. "Noncircular, finite aspect ratio, local equilibrium model". In: <u>Physics of Plasmas</u> 5.4 (1998), pp. 973–978.
- [17] M. Barnes, F. I. Parra, and M. Landreman. "stella: An operator-split, implicit–explicit  $\delta f$ -gyrokinetic code for general magnetic field configurations". In: <u>Journal of Computational Physics</u> 391 (2019), p. 365.
- [18] Rahul Gaur et al. "An adjoint-based method for optimising MHD equilibria against the infinite-n, ideal ballooning mode". In: <u>Journal of Plasma Physics</u> 89.5 (2023), p. 905890518.
- [19] C. Bourdelle et al. "Stabilizing impact of high gradient of  $\beta$  on microturbulence". In: <u>Physics of Plasmas</u> 10.7 (2003), pp. 2881–2887.